Configurable phonon polaritons in twisted α-MoO₃

M. Chen^{1†}, X. Lin^{2†}, T. Dinh³, Z. Zheng³, J. Shen¹, Q. Ma³, H. Chen², P. Jarillo-Herrero³, S. Dai¹*

¹Materials Research and Education Center, Department of Mechanical Engineering, Auburn University, Auburn, Alabama 36849, USA

²Interdisciplinary Center for Quantum Information, State Key Laboratory of Modern Optical Instrumentation, ZJU-Hangzhou Global Science and Technology Innovation Center, Zhejiang University, Hangzhou 310027, China

³Department of Physics, Massachusetts Institute of Technology, Cambridge, Massachusetts 02139, USA

†These authors contribute equally

*Correspondence to: sdai@auburn.edu

Moiré engineering is being intensely investigated as a method to tune the electronic, magnetic, and optical properties of twisted van der Waals materials. Yet these advances stem from the formation of peculiar moiré superlattices at small specific twist angles. Here we report configurable nanoscale light-matter waves – phonon polaritons – by twisting stacked α -phase molybdenum trioxide (α -MoO₃) slabs in a broad range from 0° to 90°. Our combined experimental and theoretical results reveal a variety of polariton wavefront

geometries and topological transitions as a function of the twist angle. In contrast to the origin of the modified electronic band structure in moiré superlattices, the polariton twisting configuration is attributed to the electromagnetic interaction of highly anisotropic hyperbolic polaritons in stacked α -MoO₃ slabs. These results indicate twisted α -MoO₃ as a promising platform for nanophotonic devices with tunable functionalities.

Van der Waals (vdW) structures offer a platform to design quantum materials via twisting and stacking of weakly bonded atomic layers^{1, 2}. This configuration has been recently investigated for the special case of moiré superlattices – the interference lattice pattern obtained by twisting stacked vdW materials at small angles δ – to tune the electronic, magnetic, optical, and mechanical properties of the heterostructures. Important results were first reported in electronics³⁻⁶, where moiré superlattices led to the observation of Hofstadter's butterfly, superconductivity, correlated insulating states and other exotic phases of matter. Subsequently, ferromagnetism⁷ and moiré excitons⁸⁻¹¹ were reported in vdW structures at small magic twisting angles. In nanophotonics and polaritonic nano-optics, where the research involves highly confined light-matter waves called polaritons^{12, 13}, moiré superlattices were shown to reflect plasmon polaritons in graphene¹⁴⁻¹⁷ and produce nano-light photonic crystals¹⁵.

These previous breakthroughs in configuring vdW materials remark peculiarities in the formed moiré superlattice as a special case of vdW configuration at small specific twisting angles δ (typically $\delta < 5^{\circ}$). To further exploit the advances of vdW systems, it is worth exploring the configuration of their physical properties via stacking and twisting beyond the small specific

 δ range. Yet, polaritons in vdW systems without evident moiré superlattices remain rigid for a broad range of twisting angles ($\delta > 5^{\circ}$). This lack of configurability stems from the spreading nature of polaritons in most vdW materials: once excited, the polaritons propagate toward all directions in the basal plane. The insufficient electromagnetic anisotropy of the spreading propagation weakens the twisting tunability of polaritons based on the rotation of components of the vdW system.

In this work, we report configurable phonon polaritons – light coupled to lattice vibrations – in twisted α -phase molybdenum trioxide (α -MoO₃) slabs. Different from other spreading polaritons, phonon polaritons in α -MoO₃^{18, 19} are extremely anisotropic: they propagate only along certain directions in the basal plane. Using real-space infrared (IR) nano-imaging of the propagating phonon polaritons, we demonstrated various wavefront geometries and polariton topological transitions by twisting stacked α -MoO₃ slabs with an angle δ from 0° to 90° (Fig. 1a). The phonon polariton twisting tunability originates from the electromagnetic hybridization between directional phonon polaritons in the top and bottom α -MoO₃ slab and strongly depends on the twisting angle δ . Since a variety of polariton wavefront geometries like open hyperbola and parenthesis, closed oval and squircle as well as their deformation including compression and stretching can all be achived simply by varying the twisting angle δ , twisted α -MoO₃ in this work holds promises to offer tunable IR nano-light for various nanophotonic functionalities.

The IR nano-imaging of phonon polaritons in twisted α -MoO₃ were performed using scattering-type scanning near-field optical microscopy (s-SNOM). The s-SNOM is based on a

tapping-mode atomic force microscope (AFM) which simultaneously yields the topography and nano-IR image of the scanned area (Fig. 1a). In the experiment, the AFM tip is illuminated with an IR laser (brown solid arrow) at the frequency $\omega = 1 / \lambda_0$ (λ_0 is the wavelength of IR light in free space), the topography and back scattered near-field signal (brown dashed arrow) are recorded during the scan. The experimental observable near-field amplitude $S(\omega)$ and phase $\Phi(\omega)$ typically possess a spatial resolution ~ 10 nm, close to the radius of the AFM tip, and therefore can map nano-polaritons in the real-space^{13, 14, 20}. The polaritons are typically imaged as fringes – standing wave interference oscillations – in the s-SNOM experiments.

At the IR frequency $\omega = 915 \text{ cm}^{-1}$, a representative s-SNOM amplitude $S(\omega)$ image of the single α -MoO₃ slab is shown in Fig. 1b. In the experiment, we fabricated Au disks (thickness 100 nm, diameter 1 µm) on top of the α -MoO₃ devices. The metallic Au disks can strongly concentrate electric field – the lighting rod effect²¹ – and launch^{22, 23} propagating phonon polaritons upon the IR illumination. Two types of phonon polariton fringes – the $S(\omega)$ oscillations – can be observed: "X" shape hyperbolic fringes around the Au disk (red disk) and linear fringes close to the slab edge (white dashed line). The linear fringes originate from the interference between phonon polaritons launched by the s-SNOM tip and those reflected at the crystal edges. These fringes are always parallel to the crystal edge^{22, 23} regardless of the polariton wavefront geometry. The "X" shape fringes around the Au disk are interference patterns between phonon polaritons launched by the Au disk and the IR illumination (brown solid arrow in Fig. 1a)^{22, 23}. For highly confined polaritons in vdW materials²², these fringes superposition with the

wavefront of the launched polaritons and therefore are mainly discussed in this work. In contrast to spreading concentric fringes from other vdW materials, "X" shape fringes observed in α -MoO₃ indicate the extreme anisotropy of the phonon polaritons: they propagate along certain directions. This propagation directionality stems from the hyperbolic response ($\epsilon_i \epsilon_j < 0$, where ϵ_i and ϵ_j are permittivity along different directions, i and j denote crystal axis [100], [001] or [010]) inside Reststrahlen bands of α -MoO₃^{18, 19}: Band 1 at $\omega = 542$ to 856 cm⁻¹ for [001] phonon ($\epsilon_{[100]} > 0$), $\epsilon_{[001]} < 0$ and $\epsilon_{[010]} > 0$), Band 2 at $\omega = 816$ to 976 cm⁻¹ for [100] phonon ($\epsilon_{[100]} < 0$, $\epsilon_{[001]} > 0$ and $\epsilon_{[010]} > 0$), and Band 3 at $\omega = 956$ to 1012 cm⁻¹ for [010] phonon ($\epsilon_{[100]} > 0$, $\epsilon_{[010]} > 0$ and $\epsilon_{[010]} > 0$). Specifically, the directional "X" shape fringes (Fig. 1b) are directly attributed to the basal plane hyperbolic response ($\epsilon_{[100]}\epsilon_{[001]} < 0$) inside the Reststrahlen Band 2: the isofrequency dispersion for the α -MoO₃ slab is an open hyperbola (Fig. 1c, black curve) in the basal plane and phonon polaritons propagate along fixed directions (black arrows in Fig. 1c) with an angle $\theta = arc tan \sqrt{|\epsilon_{[100]}/\epsilon_{[010]}|}$ to the [010] direction²⁴⁻²⁶.

The directional phonon polaritons in the basal plane suggest the tunability by twisting stacked α -MoO₃ slabs inside the Reststrahlen Band 2. The advance of the stacked slabs over the single slab lies at the variety of shapes and topologies of the polariton isofrequency curve that can be tuned via twisting (Fig. 1i), while the isofrequency curve in single slab is fundamentally rigid. In Figs. 1d-h, we provide s-SNOM images of phonon polaritons in twisted α -MoO₃ at various twisting angles δ . The s-SNOM images are oriented with all [001] axis of the bottom α -MoO₃ slab aligned vertically (see the coordinate axis in Figure 1). At $\delta = 0^{\circ}$, the phonon

polaritons exhibit "X" shape fringes (Fig. 1d) that correspond to the hyperbolic wavefront, very similar to that of the single slab α -MoO₃ (Fig. 1b). At $\delta = 20^{\circ}$ (Fig. 1e), the hyperbolic wavefront can still be observed but is titled from that with $\delta = 0^{\circ}$ and the single slab. The phonon polariton wavefront at $\delta = 63^{\circ}$ is different: the fringes can only be observed along a tilted line across the Au disk (Fig. 1f), the wavefront is in a parenthesis geometry, the propagation along other directions are prohibited. This parenthesis wavefront is also revealed in phonon polariton fringes launched by a defect (red * in Fig. 1f) where similar parenthesis fringes along the same direction can be observed. At $\delta = 81^{\circ}$ (Fig. 1g), the phonon polariton wavefront becomes oval, as fringes observed around the Au disk. Finally, at $\delta = 90^{\circ}$ (Fig. 1h), the wavefront appears as a squircle, rounded square phonon polariton fringes are observed. In Fig. 1h, the squircle fringes are less visible on the lower left side of the Au disk, due to the shadowing effect of the AFM cantilever²².

s-SNOM images in Fig. 1 reveal various wavefront geometries and topological transitions of the phonon polaritons in twisted α -MoO₃. As the twisting angle δ increases from 0° to 90°, the phonon polariton wavefront exhibit a hyperbola (Fig. 1d, δ = 0°), tilted hyperbola (Fig. 1e, δ = 20°), parenthesis (Fig. 1f, δ = 63°), oval (Fig. 1g, δ = 81°) and squircle (Fig. 1h, δ = 90°). Note that at $\delta \sim 63^\circ$, the phonon polariton wavefront changes from an open hyperbola-like geometry (Figs. 1d-e) to closed ellipse-like geometries (oval, squircle in Figs. 1g-h), corresponding to the topological transitions^{25, 26}. This continuous twisting tunability of phonon polariton in α -MoO₃ over the broad range δ = 0° to 90° is in stark contrast to that in twisted graphene and graphene/hBN heterostructures where plasmon polaritons are affected by the moiré

superlattice¹⁵⁻¹⁷ at specific and small twisting angles ($\delta < 5^{\circ}$).

The observed twisting tunability of phonon polariton is supported by both the finite element method (FEM) simulation and electromagnetic wave theory in Fig. 2. With the input of α-MoO₃ slab thickness and IR frequency ω from our experiment and fitted α-MoO₃ permittivity based on ref. 19, 27, we simulate the real-space electromagnetic field E_z and modelled momentum space (k-space) isofrequency dispersion in twisted α -MoO₃. In the real-space simulation (Supplementary Information S4), a vertical dipole (centers of Figs. 2a-f, top) was placed above the twisted α-MoO₃ as the polariton launcher. The real-space simulation reproduces the topological transitions of phonon polaritons in our experiment (Figure 1): the wavefront exhibit the hyperbola at the single slab and $\delta = 0^{\circ}$ (Figs 2a, b, top), tilted hyperbola at $\delta = 20^{\circ}$ (Fig. 2c, top), parenthesis at $\delta = 63^{\circ}$ (Fig. 2d, top), oval at $\delta = 81^{\circ}$ (Fig. 2e, top) and squircle at $\delta = 90^{\circ}$ (Fig. 2f, top). Our electromagnetic theory (Supplementary Information S5) of the isofrequency dispersion in twisted α-MoO₃ was developed from previous theory on black phosphorus^{28, 29} and graphene metasurface 25,30 . The modeled k-space isofrequency curves (Figs. 2a-f, bottom) are in excellent agreement with the real-space images produced in our experiment (Figure 1) and FEM simulations (Figs. 2a-f, top).

We attribute the twisting tunability reported in Figures 1-2 to electromagnetic interaction between directional phonon polaritons in the stacked top and bottom α -MoO₃ slab. Specifically, the twisting tunability requires 1) extreme basal-plane anisotropy and 2) sufficient out-of-plane field span for phonon polaritons in α -MoO₃. In Fig. 3, we provide experimental data and

calculation analysis to demonstrate these criteria for the twisting tunability. At a representative IR frequency $\omega = 980 \text{ cm}^{-1}$ in Reststrahlen Band 3, the *k*-space isofrequency curve is an ellipse (green curve, Fig. 1c) and phonon polaritons propagate with an elliptical wavefront in the real-space (Fig. 3a). Compared with directional phonon polaritons in Band 2 (Fig. 1b), phonon polaritons at $\omega = 980 \text{ cm}^{-1}$ lack sufficient anisotropy such that they spread towards all directions (Fig. 3a). The twisting tunability is ineffective at $\omega = 980 \text{ cm}^{-1}$: phonon polaritons in twisted α -MoO₃ with $\delta = 20^{\circ}$ (Fig. 3b), 63° (Fig. 3c) and 90° (Fig. 3d) all exhibit elliptical wavefront, similar to that in the single slab (Fig. 3a). These results are in stark contrast with the s-SNOM image at $\omega = 900 \text{ cm}^{-1}$ (Fig. 3f) where the squircle and a series of other wavefront (Fig. 1) can be tuned by twisting α -MoO₃ slabs.

In addition to the extreme anisotropy in the basal-plane, sufficient out-of-plane field span is also required to build adequate electromagnetic hybridization in twisted α -MoO₃ to tune phonon polaritons. Since phonon polaritons exponentially decay out-side-of the α -MoO₃ slab, this criterion corresponds to a moderate decay of the phonon polariton field. In Figure 3g, we calculated the distribution of electromagnetic field $|E_z|$ away from the α -MoO₃ slab at three representative IR frequencies: $\omega = 900$ cm⁻¹ (green) and 935 cm⁻¹ (blue) in Band 2 and $\omega = 980$ cm⁻¹ (red) in Band 3. Away from the α -MoO₃ slab, the polariton field $|E_z|$ decays quickly at $\omega = 935$ and 980 cm⁻¹ but moderately at $\omega = 900$ cm⁻¹: the field decay length where $|E_z|$ becomes 1/e of that at z = 0 is 14, 92 and 243 nm for $\omega = 980$, 935 and 900 cm⁻¹, respectively. Therefore, in the out-of-plane direction, α -MoO₃ phonon polariton field spans sufficiently at $\omega = 900$ cm⁻¹ but

insufficiently at ω = 935 and 980 cm⁻¹. In vertically stacked α -MoO₃ devices, sufficient field span of phonon polaritons from each α -MoO₃ slab leads to adequate electromagnetic interaction and thus the twisting tunability at ω = 900 cm⁻¹. Our s-SNOM data in Figs. 3d-f support this theoretical assertion. Evident twisting tunability was observed at ω = 900 cm⁻¹ (Fig. 3f and Fig. 1) while the lack of twisting configuration was observed at ω = 935 and 980 cm⁻¹. Note that at ω = 935 cm⁻¹ (Fig. 3e), the phonon polaritons in the top and bottom α -MoO₃ slab fulfill the other criterion to be anisotropic in the basal plane (hyperbolic wavefront), yet these hyperbolic modes barely interact with each other due to their insufficient out-of-plane field span (blue curve in Fig. 3g). Similar results were observed in α -MoO₃ slabs with another twisting angle at the same frequency (Supplementary Figure S3).

We emphasize that while the methodology for tuning phonon polaritons in twisted α -MoO₃ is similar to that for twistronics² in moiré engineering, their physical origins are different. The former one stems from the angle-dependent electromagnetic hybridization between anisotropic phonon polariton fields in stacked α -MoO₃, whereas the latter one is attributed to the peculiar electronic band structure modified by vdW superlattices. Therefore, phonon polaritons in twisted α -MoO₃ can be tuned via twisting in a broad range of angle δ from 0° to 90° and are relatively less sensitive on δ while twistronics is mainly investigated in vdW heterostructures at small twisting angles (typically δ < 5°) and is highly sensitive on δ . Note that the electromagnetic interaction nature of the twisting tunability of phonon polaritons was further confirmed by dispersion analysis of phonon polaritons in Supplementary Section S7.

Combined experimental and theoretical results in Figs. 1-3 report the tuning of phonon polaritons in twisted α-MoO₃. The phonon polariton wavefront can be altered by controlling the twisting angle δ between stacked α -MoO₃ slabs in a broad range of 0° to 90° , thus demonstrating the extended vdW configurability of nanoscale electromagnetic energy beyond Moiré engineering at small twisting angles²⁻⁷. The observed twisting tunability of polaritons is attributed to electromagnetic interaction between anisotropic polariton fields and is highly dependent on the twisting angle. Note that by altering the wavefront via twisting, the tuning of phonon polariton propagation direction and wavelength surpasses previous modulation efforts through refractive index engineering^{31, 32} or vdW heterostructuring³³. Future work may be guided towards exploring the dynamics and reconfigurability of twisted polariton nano-light via nano-mechanical manipulation² or vdW photonic hybrids^{1, 34, 35}. Various phonon polariton wavefront and topologies demonstrated in this work suggest the opportunity to offer polariton nano-light with tailored propagating properties and photonic density of states^{36, 37} for on-demand nanophotonic functionalities that can benefit light emission³⁷, super-Planckian thermal emission³⁸, quantum optics^{39, 40} and exotic transitions⁴¹ etc. In addition, the directional phonon polaritons, especially their collimated and diffraction-less propagation at the topological transition angle ($\delta \sim 63^{\circ}$, Fig. 3f) can be further explored for exotic nano-optical phenomena including super-Coulombic long-range dipolar interactions⁴² and others. Finally, the twisting tunability of phonon polaritons in α-MoO₃ also provides a prototype for the exploration of configuring other anisotropic physical properties in vdW materials via twisting, stacking and heterostructuring.

Note: after the submission of our paper, we became aware of two other manuscripts reporting the observation of tunable phonon polaritons in twisted van der Waals bilayers^{43, 44}.

Methods

Fabrication of twisted α-MoO₃ structures

 α -phase molybdenum trioxide (α -MoO₃) slabs were mechanically exfoliated from bulk crystals. Due to the anisotropic crystal structure, the crystallographic axes can be identified according to the long straight edge of the exfoliated α -MoO₃ slab using optical microscopy and atomic force microscopy. The stacked α -MoO₃ slabs were fabricated using the dry-transfer technique⁶. Briefly, the poly (bisphenol A carbonate) (PC)/polydimethylsiloxane (PDMS) were used to pick up exfoliated α -MoO₃ slab, rotate manually by a specific angle according to the long straight edge and stack on another α -MoO₃ slab to form twisted α -MoO₃ structures. Eelectron-beam lithography and metal thermal evaporation were exploited to fabricate small Au disk (diameter = 1 μ m, thickness = 100 nm) on the twisted α -MoO₃.

Infrared nano-imaging

The infrared nano-imaging of polaritons in twisted α-MoO₃ introduced in the main text was performed using a commercial scattering-type scanning near-field optical microscope (s-SNOM,

www.neaspec.com). The s-SNOM is based on a tapping-mode atomic force microscope (AFM). In the experiment, the AFM tip (radius ~ 10 nm, PtIr coating) was illuminated by monochromatic mid-IR quantum cascade lasers (QCLs, www.daylightsolutions.com) with a frequency coverage from 900 to 2300 cm $^{-1}$. The s-SNOM nano-images were recorded by a pseudoheterodyne interferometric detection module with an AFM tapping frequency ~ 280 kHz and tapping amplitude ~ 70 nm. The detected signal was demodulated at the third harmonics of the tapping frequency in order to obtain the pure near-field output.

Data Availability:

The data represented in Fig. 3g are provided with the paper as source data. All other data that support the findings of this study are available from the corresponding author upon reasonable request.

Code availability:

The custom code employed in this work to perform all calculations is available from the corresponding author upon reasonable request.

References:

- 1. Novoselov, K.S., Mishchenko, A., Carvalho, A. & Castro Neto, A.H. 2D materials and van der Waals heterostructures. *Science* **353**, aac9439 (2016).
- 2. Ribeiro-Palau, R. et al. Twistable electronics with dynamically rotatable heterostructures. *Science* **361**, 690-693 (2018).
- 3. Ponomarenko, L.A. et al. Cloning of Dirac fermions in graphene superlattices. *Nature* **497**, 594 (2013).

- 4. Dean, C.R. et al. Hofstadter's butterfly and the fractal quantum Hall effect in moiré superlattices. *Nature* **497**, 598 (2013).
- 5. Hunt, B. et al. Massive Dirac fermions and Hofstadter butterfly in a van der Waals heterostructure. *Science* **340**, 1427-1430 (2013).
- 6. Cao, Y. et al. Unconventional superconductivity in magic-angle graphene superlattices. *Nature* **556**, 43-50 (2018).
- 7. Sharpe, A.L. et al. Emergent ferromagnetism near three-quarters filling in twisted bilayer graphene. *Science* **365**, 605-608 (2019).
- 8. Tran, K. et al. Evidence for moiré excitons in van der Waals heterostructures. *Nature* **567**, 71-75 (2019).
- 9. Alexeev, E.M. et al. Resonantly hybridized excitons in moiré superlattices in van der Waals heterostructures. *Nature* **567**, 81-86 (2019).
- 10. Jin, C. et al. Observation of moiré excitons in WSe2/WS2 heterostructure superlattices. *Nature* **567**, 76-80 (2019).
- 11. Seyler, K.L. et al. Signatures of moiré-trapped valley excitons in MoSe2/WSe2 heterobilayers. *Nature* **567**, 66-70 (2019).
- 12. Basov, D.N., Fogler, M.M. & García de Abajo, F.J. Polaritons in van der Waals materials. *Science* **354**, aag1992 (2016).
- 13. Low, T. et al. Polaritons in layered two-dimensional materials. *Nature Materials* **16**, 182 (2016).
- 14. Ni, G.X. et al. Plasmons in graphene moiré superlattices. *Nature Materials* **14**, 1217 (2015).
- 15. Sunku, S.S. et al. Photonic crystals for nano-light in moire graphene superlattices. *Science* **362**, 1153-1156 (2018).
- 16. Jiang, L. et al. Soliton-dependent plasmon reflection at bilayer graphene domain walls. *Nature Materials* **15**, 840 (2016).
- 17. Hu, F. et al. Real-Space Imaging of the Tailored Plasmons in Twisted Bilayer Graphene. *Physical Review Letters* **119**, 247402 (2017).
- 18. Ma, W. et al. In-plane anisotropic and ultra-low-loss polaritons in a natural van der Waals crystal. *Nature* **562**, 557-562 (2018).
- 19. Zheng, Z. et al. A mid-infrared biaxial hyperbolic van der Waals crystal. *Sci Adv* 5, eaav8690 (2019).
- 20. Dai, S. et al. Tunable Phonon Polaritons in Atomically Thin van der Waals Crystals of Boron Nitride. *Science* **343**, 1125-1129 (2014).
- 21. Atkin, J.M., Berweger, S., Jones, A.C. & Raschke, M.B. Nano-optical imaging and spectroscopy of order, phases, and domains in complex solids. *Advances in Physics* **61**, 745-842 (2012).
- 22. Dai, S. et al. Efficiency of Launching Highly Confined Polaritons by Infrared Light Incident on a Hyperbolic Material. *Nano Lett* **17**, 5285-5290 (2017).
- 23. Alonso-González, P. et al. Controlling graphene plasmons with resonant metal antennas and spatial conductivity patterns. *Science* **344**, 1369-1373 (2014).

- 24. Caldwell, J.D. et al. Sub-diffractional volume-confined polaritons in the natural hyperbolic material hexagonal boron nitride. *Nat Commun* **5**, 5221 (2014).
- 25. Gomez-Diaz, J.S., Tymchenko, M. & Alù, A. Hyperbolic Plasmons and Topological Transitions Over Uniaxial Metasurfaces. *Physical Review Letters* **114**, 233901 (2015).
- 26. Krishnamoorthy, H.N., Jacob, Z., Narimanov, E., Kretzschmar, I. & Menon, V.M. Topological transitions in metamaterials. *Science* **336**, 205-209 (2012).
- 27. Álvarez-Pérez, G. et al. Infrared Permittivity of the Biaxial van der Waals Semiconductor α-MoO3 from Near- and Far-Field Correlative Studies. *Advanced Materials*, 1908176 (2020).
- 28. Renuka, M. et al. Dispersion engineering of hyperbolic plasmons in bilayer 2D materials. *Opt Lett* **43**, 5737-5740 (2018).
- 29. Nemilentsau, A., Low, T. & Hanson, G. Anisotropic 2D Materials for Tunable Hyperbolic Plasmonics. *Phys Rev Lett* **116**, 066804 (2016).
- 30. Hu, G., Krasnok, A., Mazor, Y., Qiu, C.-W. & Alù, A. Moiré Hyperbolic Metasurfaces. *Nano Letters* **20**, 3217-3224 (2020).
- 31. Chaudhary, K. et al. Engineering phonon polaritons in van der Waals heterostructures to enhance in-plane optical anisotropy. *Sci Adv* **5**, eaau7171 (2019).
- 32. Fali, A. et al. Refractive Index-Based Control of Hyperbolic Phonon-Polariton Propagation. *Nano Letters* **19**, 7725-7734 (2019).
- 33. Brar, V.W. et al. Hybrid Surface-Phonon-Plasmon Polariton Modes in Graphene/Monolayer h-BN Heterostructures. *Nano Letters* **14**, 3876-3880 (2014).
- 34. Woessner, A. et al. Highly confined low-loss plasmons in graphene—boron nitride heterostructures. *Nature Materials* **14**, 421-425 (2015).
- 35. Caldwell, J.D. et al. Atomic-scale photonic hybrids for mid-infrared and terahertz nanophotonics. *Nature Nanotechnology* **11**, 9-15 (2016).
- 36. Jacob, Z. et al. Engineering photonic density of states using metamaterials. *Applied Physics B* **100**, 215-218 (2010).
- 37. Galfsky, T., Gu, J., Narimanov, E.E. & Menon, V.M. Photonic hypercrystals for control of light-matter interactions. *Proc Natl Acad Sci U S A* **114**, 5125-5129 (2017).
- 38. Guo, Y., Cortes, C.L., Molesky, S. & Jacob, Z. Broadband super-Planckian thermal emission from hyperbolic metamaterials. *Applied Physics Letters* **101** (2012).
- 39. Hoang, T.B., Akselrod, G.M. & Mikkelsen, M.H. Ultrafast Room-Temperature Single Photon Emission from Quantum Dots Coupled to Plasmonic Nanocavities. *Nano Lett* **16**, 270-275 (2016).
- 40. Bogdanov, S.I. et al. Ultrabright Room-Temperature Sub-Nanosecond Emission from Single Nitrogen-Vacancy Centers Coupled to Nanopatch Antennas. *Nano Letters* **18**, 4837-4844 (2018).
- 41. Rivera, N., Kaminer, I., Zhen, B., Joannopoulos, J.D. & Soljacic, M. Shrinking light to allow forbidden transitions on the atomic scale. *Science* **353**, 263-269 (2016).
- 42. Newman, W.D. et al. Observation of long-range dipole-dipole interactions in hyperbolic metamaterials. *Sci Adv* **4**, eaar5278 (2018).

- 43. Hu, G. et al. in arXiv e-prints arXiv:2004.14217 (2020).
- 44. Duan, J. et al. in arXiv e-prints arXiv:2004.14599 (2020).

Acknowledgments:

We acknowledge helpful discussions with X. Jiang, J. Lin and T. Low. Work at Auburn University

was supported by the Auburn University Intramural Grants Program and National Science

Foundation under grant no. DMR-2005194. Work in the PJH group was supported through

AFOSR grant FA9550-16-1-0382 (fabrication), and the Gordon and Betty Moore Foundations

EPiQS Initiative through Grant GBMF4541 to PJH. This work made use of the Materials

Research Science and Engineering Center Shared Experimental Facilities supported by the

National Science Foundation (NSF) (Grant No. DMR-0819762). The work at Zhejiang

University was sponsored by the National Natural Science Foundation of China (NNSFC) under

Grants No. 61625502, No.11961141010, and No. 61975176, the Top-Notch Young Talents

Program of China, and the Fundamental Research Funds for the Central Universities.

Author contributions: M. C. and X. L. contributed equally to this work. S. D. conceived the

idea and designed the experiments. M. C. performed the optical experiments. T. D., Z. Z. and Q.

M. prepared the samples. X. L. and H. C. developed the theory. M. C. and J. S. performed the

simulation. M. C. and S. D. analyzed the data. M. C., S. D. and X. L. wrote the manuscript, with

input and comments from all authors. S. D., H. C. and P. J-H supervised the project.

Competing interests: The authors declare no competing interests.

16

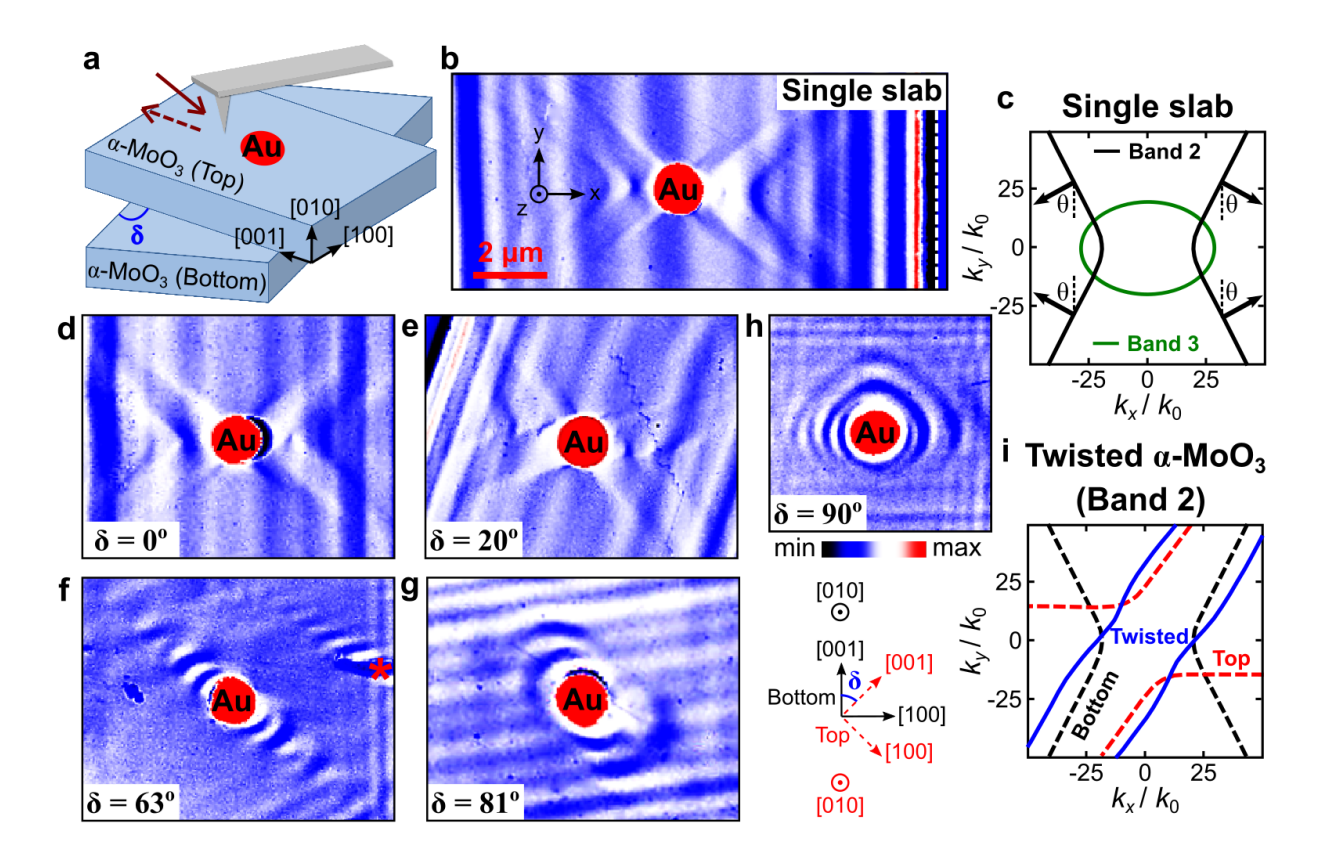


Figure 1 | Real-space IR nano-images reveal the twisting tunability for phonon polaritons. a,

Experiment schematic. Solid and dashed brown arrows denote the incident and back-scattered IR light at the AFM tip (grey). Light blue boxes denote the stacked α -MoO3 slabs with crystallographic directions and twisting angle δ indicated. **b**, s-SNOM amplitude image of single slab α -MoO3. White dashed line indicate the edge of the sample. **c**, Isofrequency curves of phonon polaritons in Reststrahlen Band 2 (black curve) and Band 3 (green curve). Black arrows indicate the direction of phonon polariton momentum with the angle θ to the vertical (y) direction. **d**-**h**, s-SNOM amplitude images of twisted α -MoO3 with δ = 0°, 20°, 63°, 81° and 90°. **i**, Isofrequency curves of the twisted α -MoO3 (blue solid curve), top (red dashed curve) and bottom (black dashed curve) α -MoO3 slab. IR frequency in (**b**): 915 cm⁻¹, (**d**): 915 cm⁻¹, (**e**): 910

cm⁻¹, (**f**): 920 cm⁻¹, (**g**): 915 cm⁻¹, (**h**): 905 cm⁻¹. Scale bar: 2 μ m. Note that while the IR frequency ω slightly various from 905 cm⁻¹ to 920 cm⁻¹ for better visibility of polariton fringes in Figure 1, the same twisting configuration and topological transitions of polaritons have been observed at the fixed frequency $\omega = 910$ cm⁻¹ (Supplementary Figure S1) and $\omega = 915$ cm⁻¹ (Supplementary Figure S2).

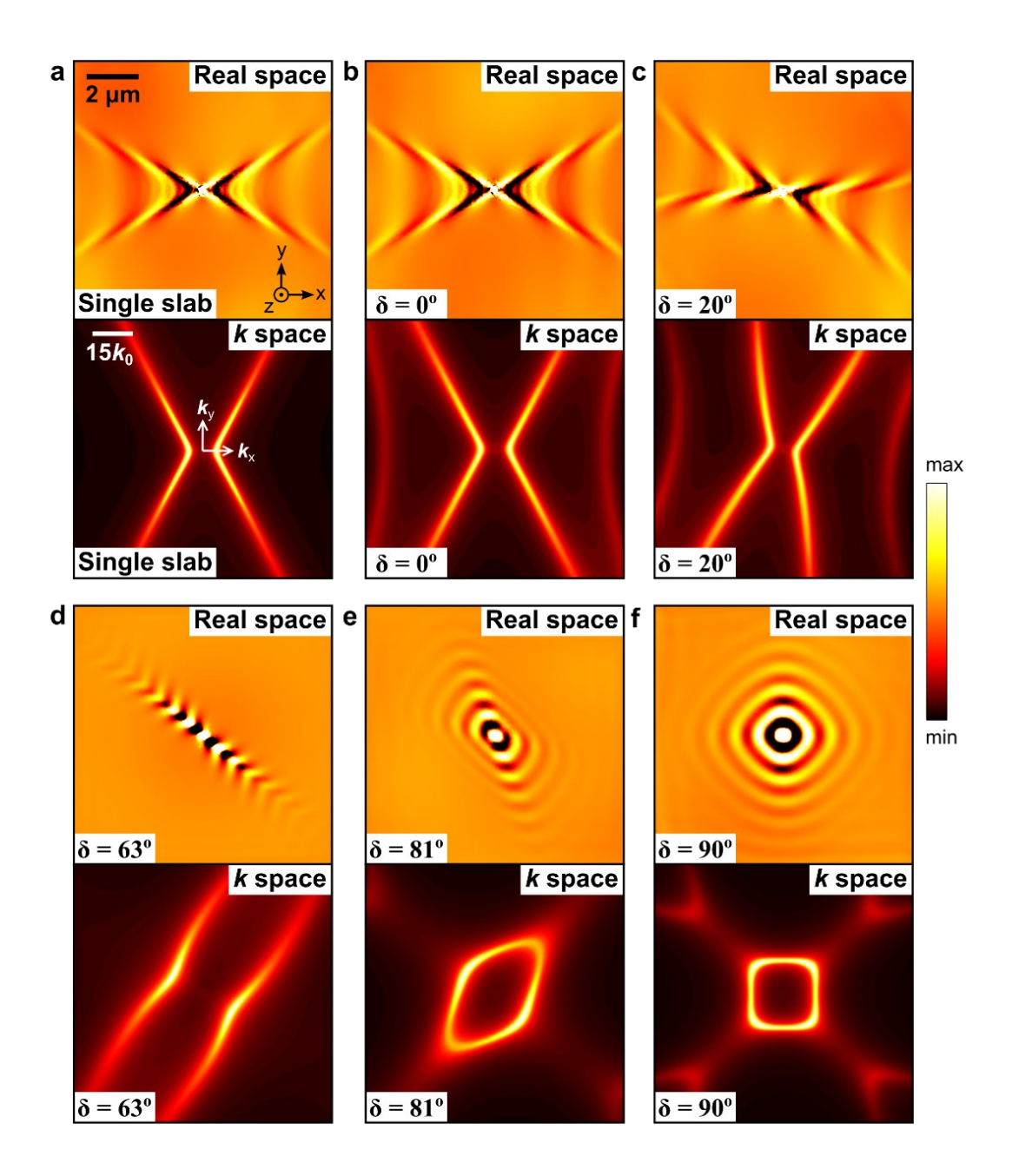


Figure 2 | Finite Element Method (FEM) real-space simulation and electromagnetic theory of momentum-space (k-space) isofrequency dispersion of phonon polaritons in twisted α -MoO₃. a–f (top), real-space FEM simulation of phonon polaritons in single slab α -MoO₃ (a) and twisted α -MoO₃ (b-f) where a dipole was placed above the center of the image to launch the

phonon polaritons. Scale bar: 2 µm. \mathbf{a} – \mathbf{f} (bottom), electromagnetic theory of corresponding isofrequency curves for single slab α -MoO₃ (\mathbf{a}) and twisted α -MoO₃ (\mathbf{b} - \mathbf{f}). Scale bar: 15 k_0 , k_0 is the momentum of IR photon $k_0 = 2\pi / \lambda_0$. Twisting angle in (\mathbf{b}): $\delta = 0^\circ$, (\mathbf{c}): $\delta = 20^\circ$, (\mathbf{d}): $\delta = 63^\circ$, (\mathbf{e}): $\delta = 81^\circ$, (\mathbf{f}): $\delta = 90^\circ$.

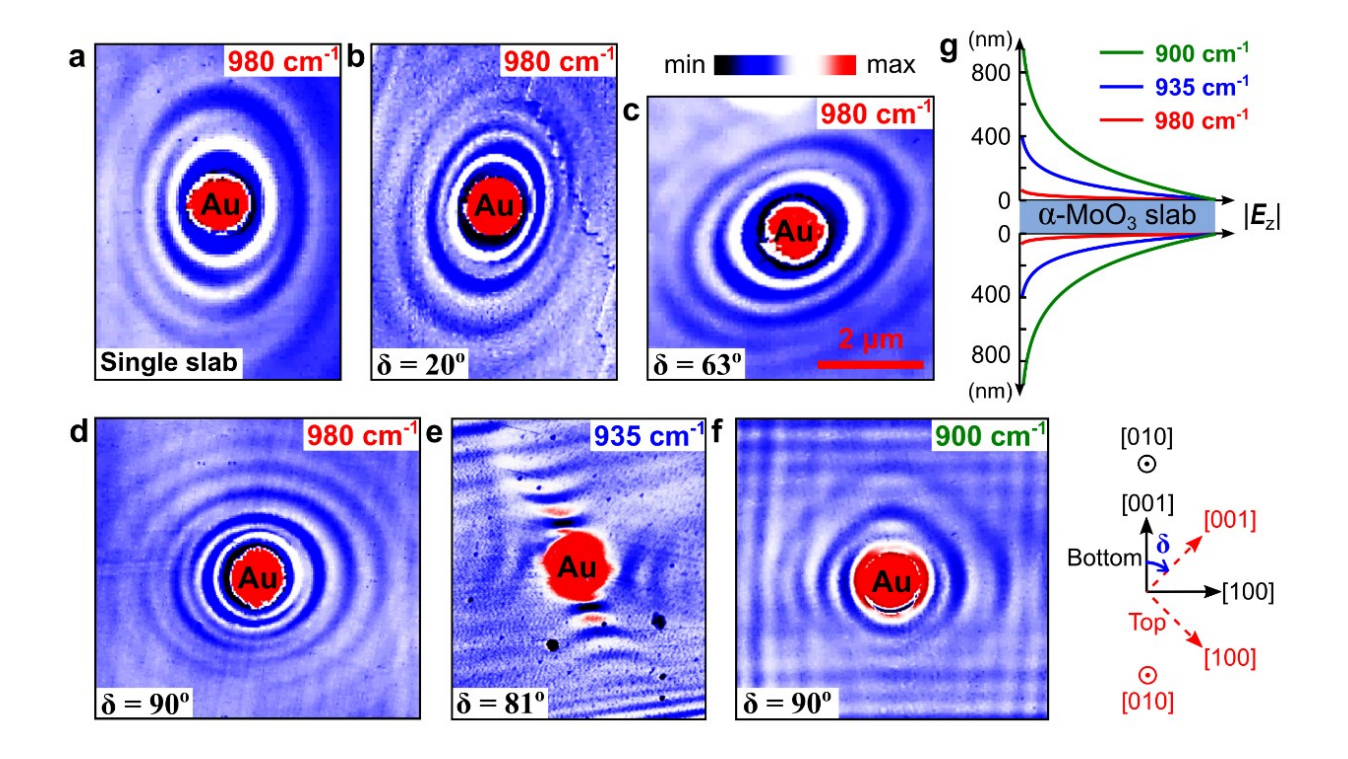


Figure 3 | Electromagnetic interaction as the origin of twisting tunability for phonon polaritons. a–d, s-SNOM amplitude images of single slab α-MoO₃ (a) and twisted α-MoO₃ with $\delta = 20^{\circ}$, 63° and 90° at IR frequency 980 cm⁻¹. e, s-SNOM amplitude images of twisted α-MoO₃ with $\delta = 81^{\circ}$ at IR frequency 935 cm⁻¹. f, s-SNOM amplitude images of twisted α-MoO₃ with $\delta = 90^{\circ}$ at IR frequency 900 cm⁻¹. Scale bar: 2 μm. g, theoretical electromagnetic field distribution | E_z | (horizontal axis) along the [100] direction away from the α-MoO₃ slab at IR frequency $\omega = 900$ cm⁻¹ (green), 935 cm⁻¹ (blue) and 980 cm⁻¹ (red). α-MoO₃ thickness: 100 nm.